Journal of Materials and Manufacturing 4(2): 25-40 (2025)

Journal of Materials and Manufacturing

Fan shaft casting design: simulation verification and trial casting evaluation

Lemuel N. Apusaga*, Earl John T. Geraldo, Karen C. Santos, Joey G. Pangilinan, Alistaire Kerwin A. Acma, and Key T. Simfroso*

Materials and Process Research Division, Department of Science and Technology – Metals Industry Research and Development Center (DOST-MIRDC), General Santos Ave., Bicutan, 1631 Taguig City, Metro Manila, Philippines
(ORCID: 0000-0002-2491-8161), lnapusaga@mirdc.dost.gov.ph
(ORCID: 0000-0002-3078-8201), etgeraldo1@gmail.com
karencagalingan@gmail.com
(ORCID: 0000-0003-2678-9989), jgpangilinan@mirdc.dost.gov.ph
(ORCID: 0009-0007-2826-1885), akacma@mirdc.dost.gov.ph
(ORCID: 0000-0002-3066-0179), ktsimfroso@mirdc.dost.gov.ph

Abstract

A fan shaft casting design intended for high-temperature service was developed and evaluated through simulation and trial casting. Initial casting simulations using NovaFlow&Solid were conducted to identify an optimal gating and riser design for sand-casting process. A rectangular tapered sprue (52 mm × 26 mm entrance area, taper angle 1°) was employed for manufacturability and to stabilize gravity filling. Melt entry was controlled using a Weir-type pour basin (depth 100mm, Weir radius 2.5mnm) coupled with an offset dross-trap to reduce turbulence and surface oxidation. Continuous tangential gating (length 667.5 mm, thickness 12 mm, width 150 mm, 5° taper) induced a controlled vortex fill, promoting non-turbulent filling behavior while maintaining thermal segregation of hotter metal toward the top of the shaft along the gate length. Directional solidification was supported by a ~1° bottom-shaft taper and adding an exothermic sleeve feeder above the blade-shaft junction. Among four exothermic feeder sleeves evaluated simulated, the optimal riser was an exothermic sleeve (internal volume: 577,267.65 mm^3) with a 70 mm neck diameter, providing 17% utilization while eliminating shrinkage porosity at the blade root. The resulting design parameters were then applied to a no-bake molding system, where the final fan shaft was cast using SCH 15 stainless steel. The cast fan shaft was assessed through inspections, followed by sectioning to evaluate internal soundness. The casting trial results showed with most sections free from shrinkage cavities and exhibiting only minimal surface depressions. The observed deviation between the simulated and experimental casting results arises from the software's limited material database, which lacked the specific alloy employed in the actual casting trials, and also by several additional factors inherent to real casting conditions which were assumed constant during simulation. However, the final casting output demonstrated fair agreement with the simulation results which confirms the effectiveness of the molding system and the adequacy of the developed casting design for producing a sound fan shaft component.

Keywords: casting design; casting simulation; fan shaft; no-bake molding system; sand casting.

1. Introduction

Casting is one of the most practical and widely used metal-forming processes in the industry. It involves melting a metallic charge, pouring the molten metal into a mold, and letting it solidify into the required shape. This process makes it possible to produce complex components efficiently and at lower cost, without the need for excessive machines or fabrication. Because of its versatility—especially in sand casting—it remains essential for manufacturing large and intricate parts like fan shafts, impellers, housings, and pump bodies. In many industries, casting continues to be a key process not just for productivity but also for sustainability, as it allows for the reuse of scrap metal and supports more resource-efficient production [1].

* Corresponding authors
E-mail addresses: lnapusaga@mirdc.dost.gov.ph, ktsimfroso@mirdc.dost.gov.ph
DOI: 10.5281/zenodo.18062212
Received: 10 November 2025, Revised: 15 December 2025, Accepted: 24 December 2025
ISSN: 2822-6054

In any casting process, the way molten metal flows, cools, and solidifies directly affects the final quality of the product. Common issues such as shrinkage porosity, misruns, cold shuts, and gas inclusions usually come from poor gating or riser design, or improper feeding during solidification [2]. These defects can impact the mechanical strength of components, especially rotating parts like fan shafts that are exposed to continuous stress and high temperatures. Because of this, it is important to control and optimize casting parameters to achieve good metallurgical quality and dimensional accuracy.

With the help of modern casting simulation software, foundries today can predict how molten metal behaves even before production starts. Programs like NovaFlow & Solid (NovaCast), MAGMASoft, and ProCAST allow engineers to visualize metal flow, heat transfer, and solidification patterns to identify where defects might form [3]. By simulating the process, it is possible to adjust casting parameters such as gating and riser design, pouring temperature, and cooling rate to minimize errors. This reduces material waste, shortens trial runs, and improves overall yield and process consistency.

According to Jin, 2025, optimizing sand-casting parameters through simulation can help eliminate unfilled regions and reduce shrinkage by improving feeding and solidification of uniformity [4]. His simulation-based design for a geometrically complex backward-curved fan produced a defect-free casting, with mechanical performance showing negligible deformation and stress that validated the approach. Likewise, Sultana et al., 2019 showed that using casting simulation together with actual validation tests improves defect prediction accuracy and aligns well with real microstructural results [1]. In their work, experimental trials confirmed that a proposed gating and feeding design for an aluminum flywheel improved casting yield by approximately 15% compared with conventional practice. Anggono et al., 2020 also reported a casting design, simulation and manufacturing validation of air compressor fan blade, establishing that defects are predictable and that process and design improvements can be finalized ahead of actual casting [5]. More recently, Patwari et al., 2024 also found that combining manual and digital optimization techniques in casting improve reliability and product quality [6]. These studies clearly show how simulation-based design connects computational modeling with actual foundry performance. Most studies that integrate manual and digital approaches in casting primarily focus on symmetric metal components such as fans, impellers, and similar geometries [5, 7-9]. However, to date, there is a notable lack of literature addressing the casting of fan-like components featuring very thin blades attached to a long, slender rod which poses a complex type of component. Casting, whether conducted manually or through simulation, remains highly dependent on practitioner expertise, and producing this type of metal component is quite challenging.

This study focuses on the design and development of a fan shaft casting intended for high-temperature service. The selected material, SCH 15 stainless steel, is a heat-resistant alloy suitable for components exposed to oxidizing environments and mechanical stress. The work combines simulation verification and trial casting evaluation to develop a sound and defect-free component. Initial simulations using NovaFlow&Solid were carried out to refine the gating and riser design for sand-casting process. The design was applied in a no-bake, Furan in particular, molding system. Despite minor casting defects observed in the initial trials, the design serves as a promising foundation for further improvement through advanced simulation tools and optimized pouring parameters.

2. Methodology

2.1 *Model Generation*

Parametric CAD modeling was used to generate the 3D models and technical drawings, which served as the basis for casting, machining, and assembly. Notably, the part design features multiple diameters in a stepped fashion reaching nearly one meter in length and tapered blades going down to a thickness of 9 mm, as can be seen in Fig. 1. The combination of the long arm and relatively thin features poses a significant challenge in ensuring sound cast to meet its service requirements. The casting cavity model was designed with a 1.5% shrinkage factor and included machining allowances.

The model was then adjusted according to Fig. 2 and 3 to account for machining allowance. Noticeably, the machining allowance is larger for the end section, as this would be the determined placement for the feeder. The casting cavity model is an upscaled model of the model with machining allowance, by a 1.5% factor, to

account for the shrinkage of the material as common practice by the foundry for steel alloy casts. This casting allowance was also adopted by the researchers for this product development and was applied when making the pattern.

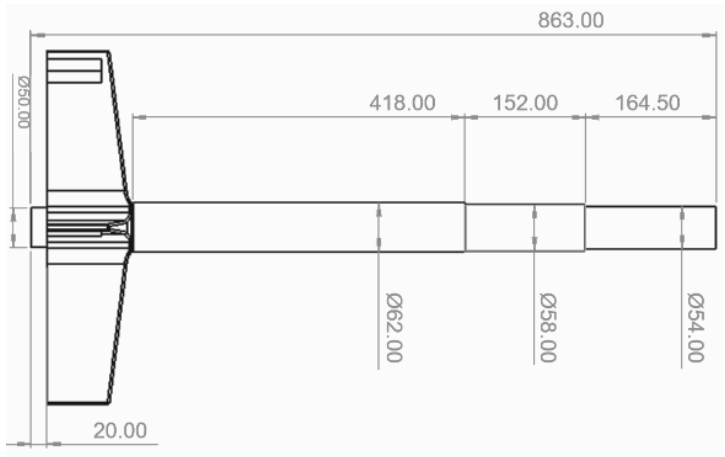

Fig. 1. CAD model and dimensional drawing of the fan shaft, showing stepped diameter transitions, along the shaft body, and blade sections with a minimum thickness of 9 mm.

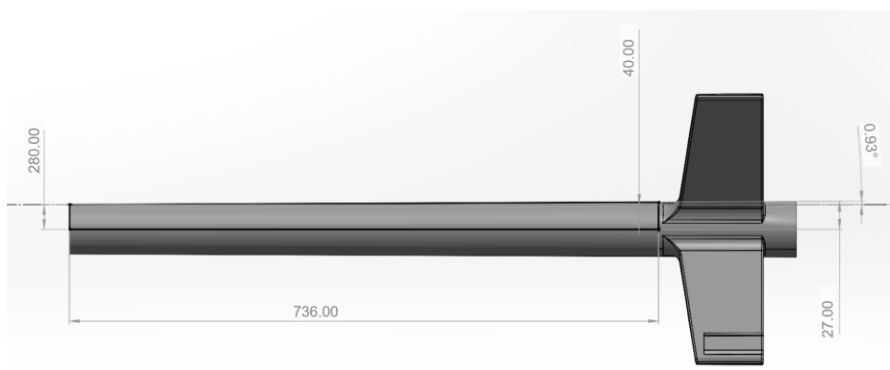

Fig. 2. Adjusted casting model incorporating machining allowance.

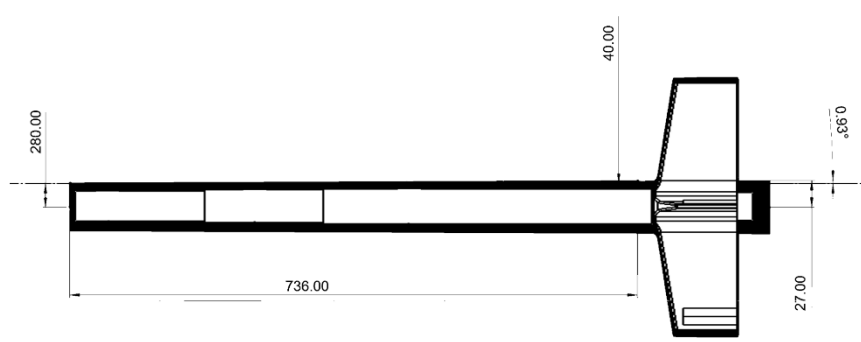

Fig. 3. Overlay of actual part (light area) to design with machining allowance (shaded area).

2.2 *Casting Design and Simulation*

The supposed fabrication of the fan shaft is to cast SCH 15 stainless steel, with its chemical composition presented in Table 1, along with the report of the metal composition used during the cast. The casting simulation was conducted using NovaFlow&Solid 6.5 Release 3 software. However, as the version employed was an educational license with a limited material database, the specific grade SCH 15 was not available. SCH 15 is a Japanese Industrial Standards (JIS) G5122 specification and an equivalent alloy under the DIN (German Institute of Standardization or "*Deutsches Institut für Normung*") standard is the GX40CrNiSiNb38-18 [10,11]. To approximate its behavior in the simulation, the alloy GX40CrNiSiNb38-19—chosen for its closely comparable chemical, physical, and mechanical characteristics [12,13]—was selected as an alternative material. Its corresponding chemical composition and relevant properties are presented in Table 2.

Table 1. Chemical composition, physical and mechanical properties of SCH 15.

Chemical Composition				Physical and Mechanical Properties			
Element	Range	Actual	Remarks	Properties	Physical	Mechanical	
C	0.35 – 0.70	0.048	Pass	Tensile strength	115-234	231-231	σb/MPa
Si	2.5 max	0.416	Pass	Yield strength	23	15	σ 0.2 ≥/MPa
Mn	2.0 max	0.527	Pass	Elongation	65	56	δ5 ≥ (%)
P	0.04 max	0.0023	Pass				
S	0.04 max	<0.0010	Pass				
Cr	15.0 – 19.0	15.86	Pass				
Ni	33.0 – 37.0	33.25	Pass				
Mo		0.126					
Al		0.0129					
Co		0.112					
Cu		0.0858					
Ti		0.0100					
V		0.0431					

Table 2. Chemical composition, physical and mechanical properties of GX40CrNiSiNb38-19.

Chemical Composition		Physical and Mechanical Properties			
Element	Composition	Properties	Physical	Mechanical	
Fe	38.09	Tensile strength	115-234	231-231	σb/MPa
Ni	37.50	Yield strength	23	15	σ 0.2 ≥/MPa
Cr	19.50	Elongation	65	56	δ5 ≥ (%)
Si	1.70				
Mn	1.00				
C	0.40				
Mo	0.25				
Nb	1.50				
P	0.035				
S	0.025				

The simulation setup began with importing the 3D model of the casting design, which included all essential appendages such as the sprue, runners, ingates, feeders, and vents. Additional components, including exothermic sleeves, chills, and filters, were incorporated as required. After importing the necessary geometries, the gravity direction was defined, and a mold box representing the cavity boundaries was generated as shown in Fig. 4.

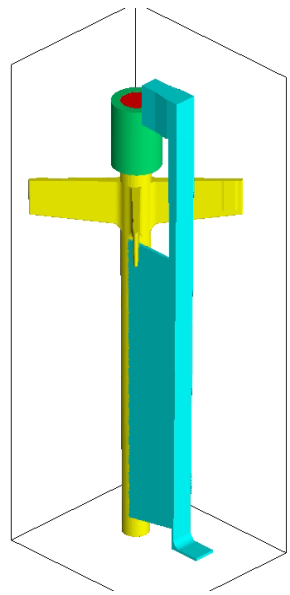

Fig. 4. Simulation setup displaying the complete casting geometry, added feeding and gating elements, and the defined mold box and gravity direction, as defined by orientation.

Thermal boundary conditions were specified for different material interfaces, namely casting-to-mold, casting-to-atmosphere, and mold-to-atmosphere interactions, illustrated in Fig 5. These boundary conditions are used by the software to facilitate interactions between the different materials. Additionally, a casting-to-atmosphere zone was manually added to the riser metal since it is not on the same height plane as the basin. The mesh size was selected to achieve an optimal balance between computational accuracy and simulation efficiency. A minimum of three mesh cells at the smallest feature is maintained throughout the iterations. This is done as a general rule of thumb for meshing, as recommended by NovaCast. After the setup of materials, the resulting mesh model was then used to define the casting process simulation parameters, which are summarized in Table 3.

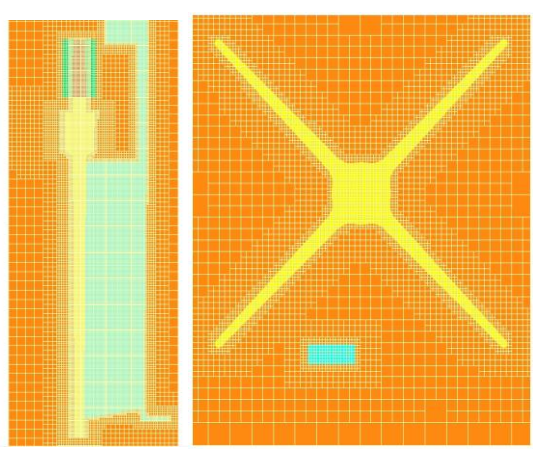

Fig. 5. Cross-section of mold (orange), fan shaft (yellow), gate system (light blue), riser (green) and feeder metal (red) showing the mesh cells efficiency.

Table 3. Material simulation parameters.

Solid Names	Materials	Temperature (ºC)
Fan shaft	GX40CrNiSINb38-19	1650.00
Mold material	Core – Furane Sand	24.00
Cavity medium	Air – In mold	20.00

Throughout the simulation, a real-time graphical interface enabled monitoring of key variables such as temperature distribution, solidification behavior, shrinkage formation, and defect prediction which facilitates iterative improvements to the casting design. Once an acceptable design was determined, the corresponding tooling was fabricated, and the process proceeded to the trial casting stage.

2.3 *Casting Process*

The molten metal used for casting was prepared using an induction furnace, which provided precise temperature control and uniform melting. The temperature of the molten metal was monitored using both an infrared thermometer and a dip pyrometer to ensure measurement accuracy and consistency. Once the target tapping temperature was achieved, the molten metal was carefully poured into the prepared molds to minimize turbulence and potential oxidation during filling. The poured metal was measured with the infrared thermometer.

For the fan shaft casting, a purely no-bake molding system was employed during the trial casting process. The no-bake mold was prepared in accordance with the standard procedure described in Ref. [14] using sand mold. The minimum mold thickness is 25 mm. The casting was conducted by pouring SCH 15 stainless steel. A total of four casting trials were conducted. In the first three trials, pouring was performed at the target temperature of 1650°C, with controlled variations to evaluate the effect of using an alloy different from that assumed in the simulation. The fourth trial incorporated insights from the initial trials to improve the casting of the fan shaft. For this trial, four molds were prepared, each assigned a specific pouring temperature: 1590°C for Mold 1, 1580°C for Mold 2, 1570°C for Mold 3, and 1560°C for Mold 4. Fig. 6 and 7 show the molding system used during these trials. The resulting fan shaft casting featured thin sections and an overall length of nearly one meter.

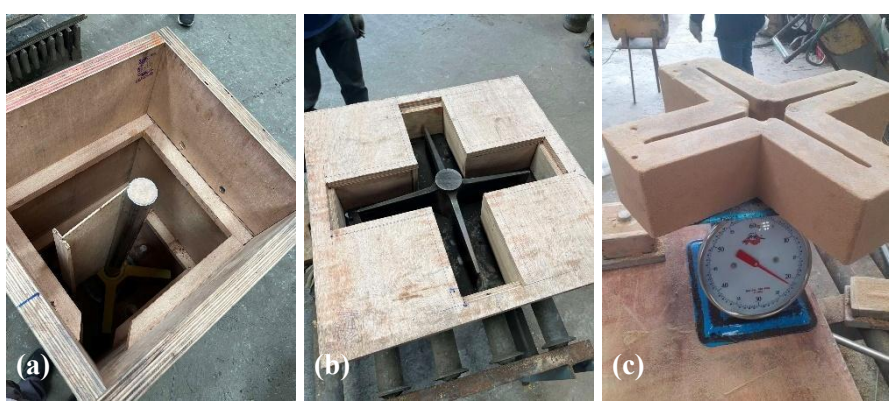

Fig. 6. Flask and no-bake molding setup: (a) flask containing the fan shaft pattern: a pattern for part of the rectangular sprue and the continuous runner gate pattern positioned tangentially to the shaft; (b) no-bake blade shaft junction mold pattern; and (c) molded blade shaft junction.

Fig. 7. Final mold assemblies for casting trials: (a) closed mold assembly highlighting the structural interfaces between shaft body, blade junction and feeder neck; (b) pouring cup with sprue extension positioned to support gravity filling and exothermic sleeve fitted; and (c) mold fitted with counterweight for stability during pouring.

2.4 *Evaluation of Cast Fan Shaft*

The cast fan shaft was assessed through a combination of visual inspection and physical verification to determine whether the component was successfully produced according to the simulation-driven mold and process design. First, the as-cast surface was examined to identify any apparent defects such as misruns, surface porosity, cold shuts, or shrinkage indications. Following this, the machining allowance along the shaft margin was removed to expose the underlying material and to confirm that the final geometry conformed to the intended design generated by the casting simulation.

To further validate internal soundness, the shaft was sectioned at selected locations. These cross-sections were examined to check whether the internal features and solidification patterns were consistent with the predicted simulation results, particularly in regions where higher thermal gradients or defect risks were anticipated.

This evaluation focused primarily on qualitative and geometry-based verification. Mechanical characterization, such as hardness testing, surface roughness measurements, tensile testing, or other quantitative assessments, was not conducted as part of the trials. This constitutes one of the limitations of the present work, since the absence of post-casting mechanical measurements prevents a more comprehensive assessment of the material's performance relative to the simulation predictions.

3. Results and Discussion

3.1 *Simulation Results*

Fig. 8 presents the casting design of the fan shaft, developed through iterative modeling and casting simulation. The simulation was split into two parts for calculation efficiency, a filling simulation and a solidification simulation. For filling simulation, the basin, sprue, and gate design was investigated and iterated. The design and filling simulation goal was for a non-turbulent metal flow into the part body, while ensuring that the hotter metal would fill up the height of the shaft to slow down the solidification along the blades. This was achieved with the uprunner thin gate that is tangentially connected along the length of the shaft. This helped with smoothing the flow of metal since the high entry speed was redirected into a vortex that slowly fills up the shaft. The waterfall effect was also minimal. A Weir type pouring basin was also utilized with a depth of 100mm and Weir radius of 2.5mm to ensure smooth entry down the sprue and minimizes trapped air once the sprue is filled. The sprue was set to be rectangular, for ease of fabrication, with dimensions 52mm by 26mm and tapered by 1° along the length. The solidification model is where the feeding system was iterated until the final design (including the exothermic sleeve) was determined. The results of the casting simulations for various design configurations were evaluated, and the optimal design was identified as the one exhibiting the casting defects.

The primary casting defects encountered during the iterations considered included shrinkage cavities, hot and cold tears, and cold laps. The most common defect encountered is the isolated shrinkage field in the blade-shaft junction due to early closing off of the feeder shaft interface before the blade-shaft hotspot is fully fed. To resolve this issue, a ~1° taper along the shaft was introduced to induce directional solidification from the bottom thinner cross-section upward and exothermic sleeves were incorporated. Four (4) available sizes of exothermic sleeves, as listed in Table 4, were examined to evaluate their effectiveness in minimizing shrinkage porosity. After several design iterations exploring different taper degrees, fan shaft orientation, feeding system designs and feeder placements, the design shown in Fig. 8 successfully eliminated the centerline shrinkage porosities below the blades.

Table 4. Volume calculations conducted comparing sleeve volume and sleeve neck diameter to keep it close to the original riser dimensions.

Sleeve No.	Original riser volume (mm^3)	Exothermic sleeve volume (mm^3)	Feeder volume vs original (%)	Fan shaft diameter (mm)	Neck diameter of sleeve (mm)
1	1,064,100.05	995,492.17	93.55%	67.45	65
2		577,267.65	54.25%		70
3		1,428,714.06	134.27%		50
4		773,460.11	72.69%		40

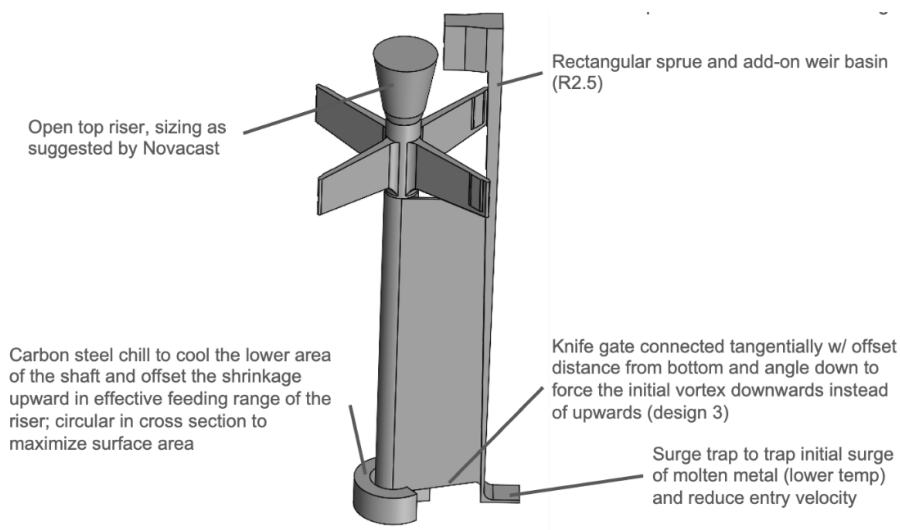

Fig. 8. Final fan shaft casting design derived from iterative simulations, showing the sprue, runner, dross trap, and riser layout used for gravity-fed pouring.

The design utilized exothermic sleeves, where Fig. 9 and 10 illustrate the solidification simulation and fullness using various sizes of sleeves. As illustrated, the shrinkage was completely eliminated from the blade junction, with sleeve no. 1 showing approximately 15% utilization of the riser volume. Exothermic sleeve no. 2, similar to sleeve no. 1, showed no shrinkage at the junction. Sleeve no. 2 was smaller by 42% in volume and had a larger neck diameter. Fullness, however, was still at 83.092% or approximately 17% utilization, indicating that a smaller-volume exothermic sleeve was still acceptable. Sleeve no. 3, on the other hand, showed a shrinkage of about 0.1% by volume, which might have been attributed to the smaller neck diameter that caused pinching of the molten metal at the riser–part junction. Exothermic sleeve no. 4 introduced more shrinkage at the junction compared to sleeve no. 3, which was due to a more drastic diameter difference between the feeder

neck and the shaft-to-riser junction. Based on these observations, sleeve no. 2 was used during the casting and simulation process.

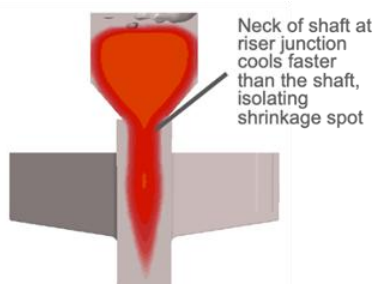

Fig. 9. Solidification simulation result from NovaCast illustrating temperature-driven progressive solidification of the shaft and blade geometry when exothermic feeding sleeve no. 4 is applied. The diameter mismatch between the feeder and contributed to the simulated isolated shrinkage field in the blade-shaft junction.

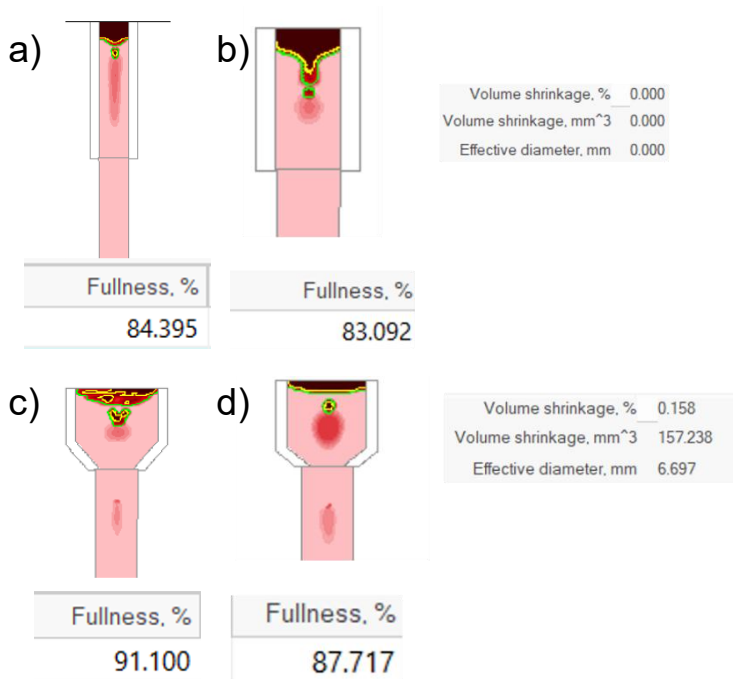

Fig. 10. Designs with exothermic sleeves (a) no. 1, (b) no. 2, (c) no. 3, and (d) no. 4 and the respective amount of metal remaining (by % volume).

3.2 *Trial Castings Results*

Trial casts were conducted using the no-bake molding system, and each cast specimen is then inspected. External defects were considered acceptable if within the casting allowance, while internal defects are all unacceptable. For internal defects, the cast fan shaft specimen is sectioned and checked for internal shrinkages. While other non-destructive scanning methods exist, sectioning was deemed more practical and economical for product development. A total of four trial casts were conducted, as was the resource available for the project. The first three trial casts yielded no successful specimen and is summarized in Table 5.

Table 5. Volume calculations conducted comparing sleeve volume and sleeve neck diameter to keep it as close to the original riser dimensions.

Trial Cast Batch No.	Specimen No.	Target Cast Temperature	Actual Cast Temperature	Findings
1	1	1650°C	1652°C	Shrinkage field extends in a column through majority of shaft length; Feeder metal was consumed more than simulation; Rough surface finish
2	1	1550°C	1550°C	Shrinkage field extending through upper portion of shaft length but significantly less than first batch of cast; Exothermic sleeve bumped to next size; Improvement in mold coating system provided smoother surface finish
3	1	1640°C	1631°C	Riser shrinkage extends up to part from the riser; Feeder metal behavior consistent with batch 2; Surface finish consistent with batch 2
	2	1630°C	1631°C	Riser shrinkage extends up to part from the riser
	3	1620°C	1624°C	Mold failure causing metal runout
	4	1580°C	1573°C	Riser shrinkage extends up to part from the riser but only until the blade junction

It was noted that temperatures close to the design simulation temperature (1650°C) consistently featured a shrinkage column that extended through majority of the shaft length. Hence, the temperatures close to 1570°C were thought to yield better casts and were used for the final trial cast batch. A simulation study was also conducted for the temperatures 1560°C, 1570°C, 1580°C, and 1590°C however the results show internal shrinkage at the blade-shaft junction, illustrated in Fig. 11, of approximately 0.01% (by total part volume) for this range. This is in comparison to the simulation at 1650°C which showed no shrinkage field at the same junction. From these observations, four (4) specimens were cast in the last trial under different pouring temperatures, with target temperatures of 1590°C (Specimen 1), 1580°C (Specimen 2), 1570°C (Specimen 3) and 1560°C (Specimen 4), each in a separate mold. Fig. 12-16 show the resulting fan shaft samples and their corresponding evaluations based on surface finish inspection and sectioning analysis.

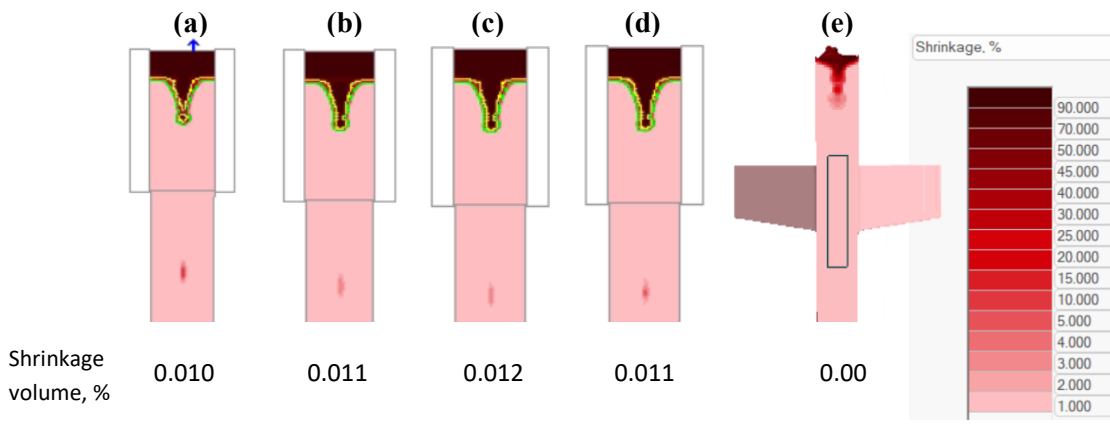

Fig. 11. Simulation results at (a) 1560°C, (b) 1570°C, (c) 1580°C, (d) 1590°C and (e) 1650°C, showing their respective shrinkage volume in %.

3.2.1 Specimen 1

The specimen cast at an actual pouring temperature of 1591°C (target: 1590°C) shown in Fig. 12 and 13 exhibited a uniform and smooth surface, indicating favorable mold-metal interaction during pouring and solidification. The smooth surface is a qualitative comparison to previous trial casts, where the surface gets

rougher along the surface of the shaft. A smoother cast surface is favorable to preserve machine tool life, while a rougher surface finish would have to be ground manually to improve surface machinability. The improvement is due to a process change which allowed the mold slip coating to reach the inner mold surfaces more uniformly. The no-bake mold coating system proved effective in minimizing metal penetration and surface-related defects, thereby ensuring a sound surface condition. The feeding system also performed satisfactorily, as evidenced by the riser shrinkage pipe not extending into the casting region, which suggests that the molten metal flow and solidification fronts were well balanced to prevent shrinkage defects in critical areas. However, after partial machining, a localized shrinkage porosity was detected at the outer rim of the base, likely originating from a region of insufficient feeding or delayed solidification. This porosity was fully removed during final machining, resulting in a sound, defect-free component suitable for subsequent evaluation and assembly.

Fig. 12. Specimen from trial cast batch 1 showing surface quality degradation along the shaft length. Section taken from the middle of the shaft (left) and the end of the shaft (right).

Fig. 13. Casting trial specimen 1 produced at an actual pouring temperature of 1591 °C: (a) as-cast component exhibiting uniform surface finish and minimal metal-mold interaction defects; (b) pre-machining condition after riser removal; and (c) partially machined section revealing a shallow peripheral shrinkage porosity associated with localized feeding deficiency during final solidification.

3.2.2 Specimen 2

The specimen shown in Fig. 14 cast at an actual temperature of 1578°C of the supposed 1580°C pouring temperature. This may result from heat losses during metal transfer, delays between furnace tapping and pouring, or thermal interactions with the ladle or pouring equipment. The cast specimen also exhibited a satisfactory surface finish, which suggests stable metal flow and proper mold coating performance under this pouring temperature. The coating effectively prevented surface reactions and metal penetration resulting in a clean and well-defined casting surface. Similar to Specimen 1, the riser shrinkage pipe did not extend into the casting region. However, during partial machining, an isolated shrinkage field was revealed, likely originating from a localized region with insufficient feeding or reduced thermal gradients. This observation suggests the

presence of minor internal porosity that may be mitigated through further optimization of the riser design or pouring temperature.

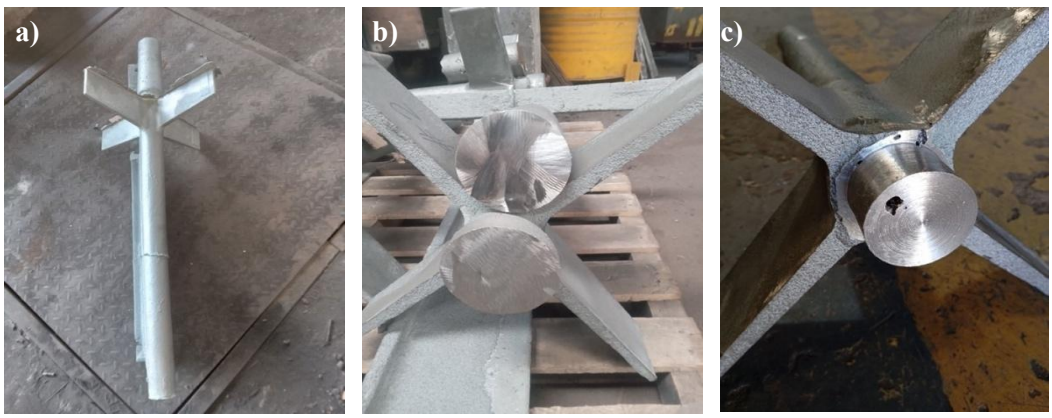

Fig. 14. Casting trial specimen 2 produced at an actual pouring temperature of 1578 °C: (a) as-cast morphology showing uniform surface topology; (b) pre-machining condition following riser removal; and (c) partial machining revealing a localized shrinkage field indicative of insufficient feeding in a confined thermal-gradient zone.

3.2.3 Specimen 3

Specimen 3 was intended to be cast at a target pouring temperature of 1570°C; however, the actual measured temperature was 1578°C. The temperature deviation may be attributed to furnace thermal overshoot, which occurs when the heating system continues to supply heat even after the set point is reached due to the response lag in the control system. Shown in Fig. 15 is the specimen 3 which also exhibited a refined surface texture comparable to the other samples produced in this casting trial. The mold coating system effectively maintained surface integrity that minimized oxidation and metal-mold reactions during solidification. As with the previous specimens, the riser shrinkage pipe did not extend into the casting section which indicates proper feeding efficiency and stable solidification behavior. Upon partial machining, however, a shrinkage porosity was detected near the periphery of the base as illustrated in Fig. 15(c). Similar to the observation in Specimen 1, this porosity was shallow and confined near the surface which suggests it originated from a localized thermal contraction zone during the final stages of solidification. The defect was expected to be completely removed during final machining, yielding a structurally sound component.

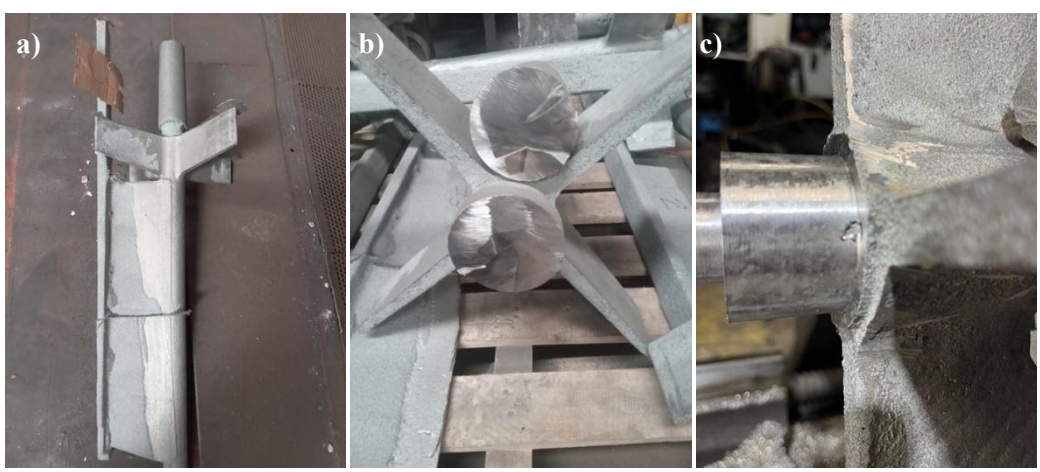

Fig. 15. Casting trial specimen 3 (actual pouring temperature: 1578 °C): (a) as-cast surface condition; (b) pre-machining state after initial cleaning; and (c) partially machined surface exhibiting shallow peripheral shrinkage porosity associated with late-stage solidification contraction at the base region.

3.2.4 Specimen 4

The specimen 4 was cast at an actual pouring temperature of 1564°C (target: 1560°C) and Fig. 16 shows the as cast sample. Similar to specimen 3, the shrinkage field of the feeder did not reach the part and machining of the specimen showed no shrinkage fields. Fig. 18 shows the sectioned feeders of the different samples. Large shrinkage cavities and internal porosities are visible in several sections, particularly in Specimens 1, 3 and 4, with Specimen 4 having the most shrinkage within the feeder while not reaching the part itself.

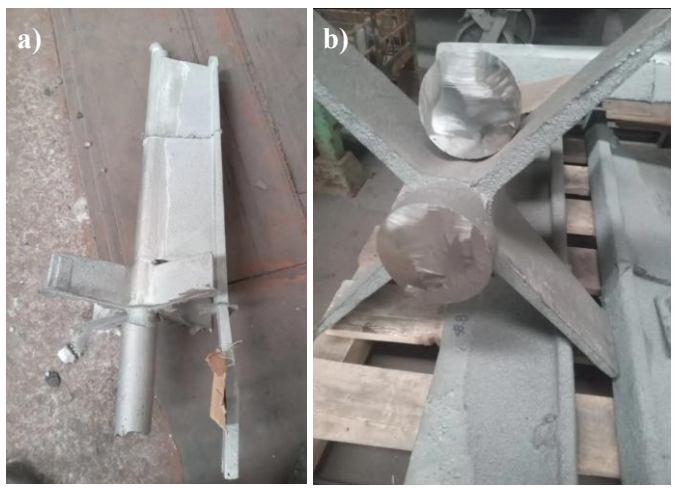

Fig. 16. Casting trial specimen 4 (actual pouring temperature: 1564 °C): (a) as-cast surface condition; (b) pre-machining state after initial cleaning showing absence of shrinkage field from the feeder.

3.2.5 Sectioning Analysis and Assessment of Casting Performance

Fig. 17 and 18 present the sectioned cast fan shaft body of the Specimen 1-3 and 4, respectively. The irregular morphology of the shrinkage cavities further points to non-directional solidification, implying that some critical regions may have solidified prematurely. Such early freezing can cut off feeding paths, resulting in void formation and non-uniform internal density. Although the shrinkage did not reach the fan shaft, a lower casting temperature would likely have posed significant problems by introducing internal defects that compromise the structural reliability of the fan shaft.

Fig. 17. Sectioned evaluation of the feeders of the fan shaft specimen cast at (a) 1578°C [specimen 2, target: 1580°C], (b) 1578°C [specimen 3, target: 1570°C], and (c) 1591°C [specimen 1, target: 1590°C]. Specimen 2 and specimen 3 show similar feeder utilization despite having different results, considering both specimens were cast at the same pouring temperature.

Fig. 18. Sectioned evaluation of the feeder of casting trial specimen 4 (actual pouring temperature: 1564°C; 1 – top section, 5 – feeder-shaft-interfacing section): (a) external surfaces of the sectioned samples showing overall surface integrity; (b) upper cross-sections revealing extensive interdendritic shrinkage cavities and centrally concentrated feeding-related porosity; and (c) lower cross-sections showing partial soundness in distal regions, particularly to the section closest to the shaft.

The deviation observed between the simulation and experimental results is likely influenced not only by the limitations of the software's material database but also by several additional factors inherent to real casting conditions. The simulation assumes fixed values for parameters such as mold thermal conductivity, a stable and uniform pouring process, and constant boundary conditions. In practice, however, these factors vary significantly during casting. For example, the actual thermal conductivity of the mold can change depending on the sand type, moisture content, binder distribution, and degree of compaction, all of which affect heat transfer and solidification behavior. Similarly, slight fluctuations in pouring temperature, flow rate, and turbulence are unavoidable during metal transfer and can alter the initial thermal conditions. Furthermore, boundary conditions, particularly the mold-metal interface heat transfer coefficient, are not constant in real processes and evolve dynamically during filling and early solidification. These differences between actual casting conditions and the simplified assumptions used in the simulation contribute to the discrepancies observed in the results.

Overall, the results indicate that the casting trial was only partially successful. While the external geometry and surface quality were achieved, the internal shrinkage porosity highlights the difference between initial simulated casting temperature (1650°) compared to the actual cast temperature used that yielded successful results (1560°C to 1590°C). The design can also use further refinement of the riser configuration, feeding system layout, and the pouring temperature. Optimizing these parameters are necessary to improve the yield by lowering reject rate and produce a structurally sound component suitable for service conditions.

4. Conclusion

The study verified the feasibility of the fan shaft casting design through iterative simulation using casting software and experimental validation via the no-bake molding process. While the design successfully promoted directional solidification and minimized major shrinkage cavities in critical regions, the work presents several limitations. First, the simulation relied on NovaFlow&Solid 6.5 with an approximated substitute alloy GX40CrNiSiNb38-19 due to the absence of the actual material SCH 15 in the database, which contributed to deviation between predicted and experimental shrinkage behavior. Second, trial castings were limited to a narrow pouring temperature window (1560–1590 °C), and mechanical property testing (e.g., tensile strength,

hardness, or impact resistance) was not performed to fully validate service performance under high-temperature rotational stress. Lastly, feeding behavior was evaluated by sectioning and machining outcomes but did not include quantitative porosity characterization such as micro-computed tomography or density-based measurements.

Future optimization should therefore focus on: (1) repeating simulations in commercial software platforms such as ProCAST or MAGMASoft to enable accurate thermal modeling with expanded alloy databases; (2) widening experimental variables by assessing lower and higher pouring temperatures, and modifying feeding geometry by optimizing riser-neck diameter and riser volume to extend feeding distance and prevent peripheral porosity; and (3) performing mechanical property validation on final castings to verify suitability for prolonged high-temperature service. Supplementing these improvements will support higher simulation fidelity, measurable internal soundness, and full performance assurance of the developed component.

Author Contribution Statement

Conceptualization, L.N.A and E.J.T.G.; methodology, L.N.A. and E.J.T.G.; validation, L.N.A.; formal analysis, L.N.A. and E.J.T.G; investigation, L.N.A. and E.J.T.G.; resources, L.N.A., K.C.S. and E.J.T.G.; data curation, L.N.A., K.C.S. and E.J.T.G.; writing—original draft preparation, L.N.A., E.J.T.G., A.K.A.A., and K.T.S.; writing—review and editing, L.N.A., E.J.T.G., A.K.A.A., K.T.S., and J.G.P.; visualization, L.N.A. E.G.T.G., and K.T.S.; supervision, J.G.P. All authors have read and agreed to the published version of the manuscript.

Acknowledgements

The authors would like to acknowledge the support of the R&D Evaluation Committee of DOST-MIRDC and the extended help by METERCOR during the casting trials.

References

[1] Sultana, N., Rafiquzzaman, Md., Rahman, Y., & Das A. (2018). Solidification and Filling Related Defects Analysis Using Casting Simulation Technique with Experimental Validation. International Journal of Mechanical Engineering and Applications, 6(6),150-160.

[2] Ravi, B. (2013). Metal Casting: Computer-Aided Design and Analysis. PHI Learning, https://books.google.co.kr/books?id=_AZ-kckukGwC&printsec=frontcover#v=onepage&q&f=false

[3] Malik, I., Sani, A.A., & Medi, A. (2019). Study on using Casting Simulation Software for Design and Analysis of Riser Shapes in a Solidifying Casting Component. Journal of Physics: Conference Series, 1500, 012036.

[4] Jin, C.K. (2025). Casting Simulation-Based Design for Manufacturing Backward-Curved Fan with High Shape Difficulty. Metals, 15(2), 99.

[5] Anggono, A.D., Prihtiantoro, D., & Siswanto, W.A. (2020). Casting Design, Simulation and Manufacturing Validation of Air Compressor. International Journal of Mechanical & Mechatronics Engineering IJMME-IJENS, 20, 1, 181-189.

[6] Patwari, A.U., Bhuiyan, S.A., Noman, K., & Navid, W.U. (2024). Defects and remedies in casting processes: a combinatorial approach between manual and digital optimization technique for enhanced quality casting. Discover Mechanical Engineering, 3, 39.

[7] Wang, D., Dong, A., Zhu, G., Shu, D., Sun, J., Li, F., & Sun, B. (2019). Rapid casting of complex impeller based on 3D printing wax pattern and simulation optimization. The International Journal of Advanced Manufacturing Technology, 100, 2629-2635.

[8] Zhang, Y., Li, X., He, L., Ma, C., Liu, X., & Mao, Y. (2019). Research for Process on Investment Casting of Impeller Based on 3D Printing. IOP Conf. Series: Earth and Environmental Science, 332, 042047.

[9] Zhang, Y., Li, Z-Y., Zhang, L-Y., Rong, B-S., Cai, Q-H., Zhu, R-F., & Xu, Y. (2018) Simulation and Optimization for Investment Casting of Impeller Based on 3D Printing. IOP Conf. Series: Earth and Environmental Science, 186, 012016.

[10] Kennametal. (2021). Workpiece Materials Overview Listing. https://www.purdue.edu/bidc/wp-content/uploads/2021/08/ISOGrade.pdf

[11] Mitsubishi Materials Corporation. (n.d.). Material Cross Reference List. https://www.mitsubishicarbide.net/contents/mmus/enus/html/product/technical_information/information/material_5.html

[12] Steel Grades. SCH15 Data Sheet, https://www.steel-grades.com/Steel-Grades/Mould-Steel/21/9736/SCH15.pdf

[13] Steel Grades. GX40NiCrSiNb38-19 Data Sheet, https://www.steel-grades.com/Steel-Grades/Mould-Steel/21/2160/_GX40NiCrSiNb38-19_.pdf

[14] ASM Handbook (2008). Volume 15 - Casting, Chapter: No-Bake Sand Molding, 567 - 580.